Applied Surface Science 255 (2009) 9371–9375

Contents lists available at ScienceDirect

Applied Surface Science

journal homepage: www.elsevier.com/locate/apsusc

Ferromagnetism and microstructure in Fe^+-implanted ZnO

D. Wang [a], Z.Q. Chen [a,*], F. Zhou [b], W. Lu [b], M. Maekawa [c], A. Kawasuso [c]

[a] Hubei Nuclear Solid Physics Key Laboratory, Department of Physics, Wuhan University, Wuchang Luojia Hill, Wuhan 430072, PR China
[b] National Laboratory for Superconductivity, Institute of Physics and Beijing National Laboratory for Condensed Matter Physics, Chinese Academy of Sciences, PO Box 603, Beijing 100190, PR China
[c] Advanced Science Research Center, Japan Atomic Energy Agency, 1233 Watanuki, Takasaki, Gunma 370-1292, Japan

ARTICLE INFO

Article history:
Received 26 June 2009
Received in revised form 14 July 2009
Accepted 14 July 2009
Available online 22 July 2009

Keywords:
ZnO
Implantation
Ferromagnetism
Defect

ABSTRACT

Fe ions were implanted into ZnO single crystals with multiple energies between 50 and 380 keV up to a total fluence of 12.5×10^{17} cm^{-2}. The crystal quality of Fe^+ implanted ZnO was investigated by X-ray diffraction 2θ scans and ω-rocking curve measurements. The appearance of Fe related diffraction peaks after 700 °C annealing of the implanted sample indicates possibly formation of Fe nanoparticles. Superconducting quantum interference device measurements revealed ferromagnetic behavior below 250 K for both the as-implanted and post-annealed ZnO. Photoluminescence and Raman scattering as well as X-ray rocking curve measurements all indicate introduction of structural defects after Fe implantation. Some of the defects act as nonradiative recombination centers, and suppress the visible and ultraviolet (UV) emission in ZnO. These defects also break the Raman selection rule, and lead to the activation of some silent phonon modes. Annealing of the implanted sample at 700 °C causes partial recovery of the defects, however, the X-ray diffraction results of the anneal ZnO show even an improvement of the crystal quality compared with the un-implanted one. This could be attributed to the recovery of the grown-in defects in ZnO.

1. Introduction

For the emerging scientific field of spintronics [1], materials which can provide spin-polarized charge currents for spin injection into semiconductors are required. As potential candidates, diluted magnetic semiconductors (DMS) have attracted a great deal of interests. DMS are conventional semiconductors doped with transition metal (TM) or rare-earth elements which are randomly distributed on substitutional lattice sites and ferromagnetically aligned via an indirect magnetic coupling [2–4]. Spintronic devices such as spin-valve transistors, spin light-emitting diodes, non-volatile memory, logic devices, gas sensor, optical isolators and ultrafast optical switches are some of the areas of interest for introducing the ferromagnetic properties at room temperature in a semiconductor [5,6]. The III–V and II–VI DMS have attracted considerable attention because the spin-dependent magnetic phenomena can be manipulated in these low-dimensional tailored magnetic thin films for various spin-based devices to unprecedented capabilities [7].

Transition metal doped ZnO is one of the most promising DMS candidates as it is predicted to be ferromagnetic above room temperature. Dietl et al. [2] first predicated a Curie temperature of $\geq$300 K for Mn-doped p-type ZnO based on the Zener ferromagnetism model, while the theoretical work of Sato and Katayama-Yoshida [8] also reported the room temperature ferromagnetism for ZnO doped with other 3d transition metal ions such as V, Cr, Fe, Co, or Ni. The above-predicted ferromagnetism was later confirmed experimentally in Co-doped ZnO [9], V-doped ZnO [10], and Mn-doped ZnO [11]. Up to now room temperature ferromagnetism has been reported in various TM doped ZnO, such as Co [12–16], Ni [17–19], and Mn [20,21]. There are relatively fewer reports about room ferromagnetism of Fe doped ZnO [22].

Despite the successful fabrication of ferromagnetic ZnO by doping of transition metals, the origin of ferromagnetism is still under debate. Doubts exist as to whether the ferromagnetism is intrinsic [13,15–17] or extrinsic in nature [12,19]. The intrinsic ferromagnetism occurs through interactions between the local moments of the homogeneously distributed TM atoms, which substitute for the ZnO lattice constituents, while the extrinsic ferromagnetism arises from the metallic clusters or second phase such as Co clusters in Co doped ZnO [12]. It is even suggested that native defects such as V_{Zn} or V_O might also induce ferromagnetism in ZnO [23–26].

A number of approaches have been utilized to produce ZnO based DMS, among which are pulsed laser deposition [9,10,13,16–19], molecular beam epitaxy [15], magnetron sputtering [14], solid state reaction [20], and sol–gel coating methods [12]. Due to the superior radiation resistance of ZnO, ion implantation is also a

* Corresponding author.
E-mail address: chenzq@whu.edu.cn (Z.Q. Chen).

0169-4332/$ – see front matter © 2009 Elsevier B.V. All rights reserved.
doi:10.1016/j.apsusc.2009.07.038

suitable way to introduce transition metal ions into ZnO to produce the ferromagnetism [22,27–32]. This technique offers advantage of controlling the total amounts of dopants in the selected area, high reproducibility, and no limitation of the solid solubility of dopants. Nevertheless, ion implantation will inevitably introduce lattice damage, which could degrade the electrical and optical properties. They may also affect the magnetic properties of ZnO. Studies of implantation induced defects and their annealing behavior are thus necessary to achieve ferromagnetism of Fe^+-implanted ZnO. In this paper, we report the ferromagnetism in Fe^+-implanted ZnO single crystals. The clear ferromagnetism in ZnO was observed below 250 K after implantation. The introduction and recovery of implantation induced defects were also investigated by various methods.

2. Experimental

Hydrothermal-grown undoped ZnO single crystals with a single-side polished (Zn-atom terminated) surface were purchased from Hefei Kejing Materials Technology Corporation. The samples with dimension of 10 mm × 10 mm × 0.5 mm and (0 0 0 1) orientation were implanted with Fe^+ ions at room temperature using a 400 keV ion implanter. A multiple-step implantation process was performed with seven different ion energies ranging from 50 keV to 380 keV. The implantation sequence is from low to high energy. Fe^+ ions were implanted to the polished face (Zn face) of the samples. Beam flux was about 1.2×10^{13} cm^{-2} s^{-1}.The implanted ion profile was simulated by TRIM code [33] as shown in Fig. 1, which is based on the Monte Carlo method. The implantation fluence was 5×10^{16} cm^{-2}, and the actual fluence for each energy was chosen by multiplying with their respective ratio as shown in Fig. 1. The total fluence of implanted Fe^+ ions is then 1.25×10^{17} cm^{-2}. A box-like implantation profile with a thickness of about 220 nm was formed after such multiple-step implantation. The atomic density in the implanted layer is about 5×10^{21} cm^{-3}, which corresponds to a Fe concentration of about 6 at.%. After implantation, some of the samples were annealed in open air at 700 ° C for 30 min.

All the unimplanted samples, Fe ions implanted samples and thermally annealed samples were characterized by X-ray diffraction (XRD, Bruker D8 Advance) using Cu K_α radiation to investigate the structure of ZnO samples. The crystal quality was further investigated by ω-rocking curves using Bede D1 X-ray metrology. The magnetic properties were examined by a Quantum Design Magnetic Property Measurement System XL-1 using a superconducting quantum interference device (SQUID) magnetometer. Photoluminescence studies were carried out on all the samples at room temperature using the 325 nm line of a He–Cd laser as the excitation source. The laser output power was about 2 mW. Raman spectra were excited with the 515 nm line of an Ar^+ laser with a power level of about 4.8 mW arriving at the sample surface in 180° backscattering using Renishaw Confocal micro-Raman spectroscopy RM-1000. The wavenumber of Raman shift ranged from 200 to 800 cm^{-1}.

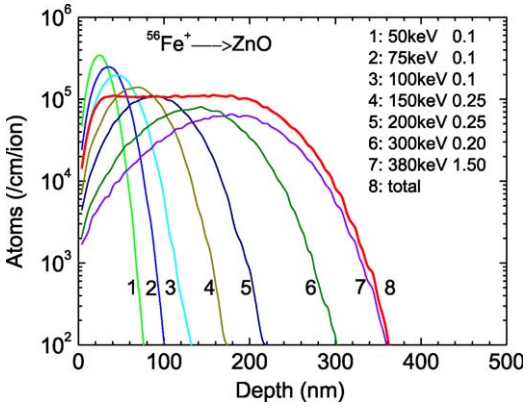

Fig. 1. TRIM simulation of the depth profile of implanted ions for the ZnO after multiple-step Fe^+ implantation.

3. Result and discussion

Fig. 2 shows the XRD patterns of ZnO before and after Fe^+ implantation and annealing. Inset of Fig. 2 shows the magnified plotting of XRD spectra in the range 2θ from 50° to 70° for thermally annealed Fe-implanted ZnO. The unimplanted ZnO single crystal has good crystallinity of wurtzite structure as evidenced by strong and sharp (0 0 2) ZnO peak at 2θ 34.4°. After Fe ions implantation, XRD scan shows a broadening of the (0 0 2) ZnO peak, which could be primarily due to the Fe^+ implantation-induced damage. The (0 0 2) peak of implanted ZnO appears at a slight lower diffraction angle compare to the ZnO single crystal. This indicates that Fe ions have been possibly diluted within the ZnO matrix, resulting in an increase of the lattice parameter of the Fe doped ZnO compared to the unimplanted ZnO. After annealing at 700 ° C for 30 min, the (0 0 2) peak becomes even sharper than that of the unimplanted one as shown in Fig. 2. Two low intensity peaks appear at 2θ 53.2° and 2θ 64.9° originating from face-centered cubic Fe (2 0 0) and body-centered cubic Fe (2 0 0) respectively as shown in the inset of Fig. 2. This indicates that most of the Fe^+ implantation-induced defects recover and two metallic secondary phases are formed due to the thermal diffusion of the implanted Fe^+ ions. This is quite different from the result of Rita et al. [34] about the thermal stability of low fluence (2×10^{13} cm^{-2}) and low-energy (60 keV) implanted Fe in bulk ZnO. They reported that Fe has superior thermal stability over other TM ions in the ZnO lattice. Most of the Fe ions are located on Zn sites even in as-implanted ZnO. Annealing at temperature lower

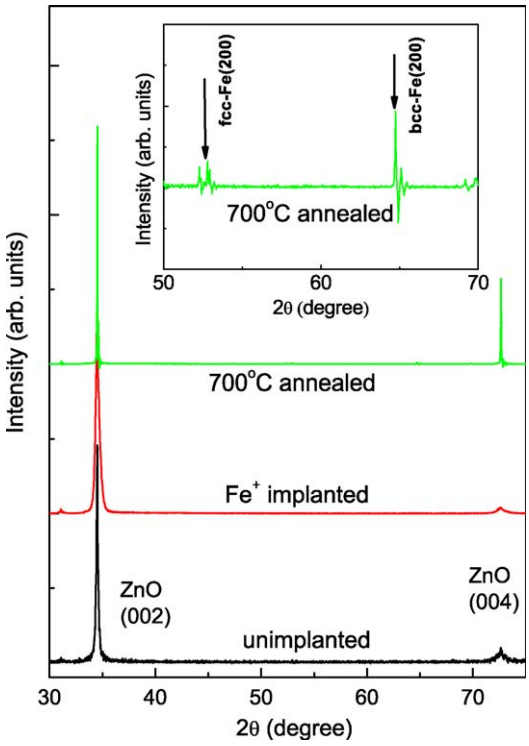

Fig. 2. The XRD 2θ scans for unimplanted ZnO, Fe ions implanted ZnO, and thermally annealed Fe-implanted ZnO. Inset: magnified plotting of XRD spectra in the range 2θ from 50° to 70° for thermally annealed Fe-implanted ZnO.

than 800 ° C does not remove the Fe ions from their substitutional sites. However, our results reveal possible Fe nanoparticle formation after 700 ° C annealing. This may be due to the higher implantation fluence in our experiment, thus the required diffusion length for nanoparticle formation becomes much shorter. The formation of such nanocrystals has been frequently reported for Co^+-implanted ZnO [27,29,32], and they are regarded as the origin of ferromagnetism in transition-metal-doped ZnO. Potzger et al. [28] and Zhou et al. [30] also observed the formation of Fe nanocrystals in Fe implanted ZnO.

Fig. 3 presents the (0 0 2) XRD ω-rocking curves obtained from unimplanted ZnO, Fe^+-implanted ZnO, and thermally annealed Fe-implanted ZnO. The peak positions of these curves are shifted to 0° for the comparison of the result. In the unimplanted ZnO single crystal, the full width at half maximum (FWHM) of the rocking curve is about 0.043°. A very close value of FWHM was previously reported by Chen et al. [35] in the hydrothermal grown ZnO single crystals. After Fe^+-implantation, the FWHM increases to 0.054° due to the defects induced by implantation. After annealing at 700 °C, the FWHM decrease to 0.027 ° which is even narrower than that of the unimplanted ZnO. The decrease of the FWHM suggests that the crystal quality is improved and becomes even better than the unimplanted state after high temperature annealing. This could be due to the reduction of the grown-in defects in ZnO crystals. Similar result was observed previously by Chen et al. [35] in the annealed ZnO single crystals. They reported a much lower FWHM value of 0.012° after annealing ZnO at 900 °C. Discrepancy between our result and the result of Ref. [35] may be due to the lower annealing temperature of 700 ° C in our experiment and also the remaining defects induced by Fe^+-implantation.

The magnetization behavior of the Fe^+-implanted ZnO was investigated by SQUID magnetization measurements. The as-obtained data from the SQUID measurements were divided by the total mass of implantation layer which was estimated from the TRIM simulation (Fig. 1). Fig. 4 shows the magnetization versus field behavior for Fe^+-implanted ZnO measured at (a) 300 K, (b) 250 K, and (c) 10 K. At room temperature, no hysteresis loop is observed in the magnetization versus field data within the resolution of the measurements. With temperature decreasing to 250 K, a hysteresis loop is observed. It shows a saturation magnetization of 2.8 emu/g at an applied field of 5000 Oe, a remnant magnetization of 0.15 emu/g, and a coercive field of 85 Oe. After lowering temperature to 10 K, the hysteresis loop becomes rather clear. The saturation magnetization increases to 3.3 emu/g at a field of 5000 Oe, while the remnant magnetization and the coercive field increase to 0.6 emu/g and 280 Oe, respectively. After annealing at 700 ° C for 30 min, the SQUID measurement was also performed at 250 K as shown in Fig. 4(d). No obvious change of magnetic behavior is observed. The annealed sample has a saturation magnetization of 2.5 emu/g at an applied field of 5000 Oe, a remnant magnetization of 0.14 emu/g, and a coercive field of 85 Oe. Considering the X-ray diffraction measurements, the appearance of Fe nanoparticles after 700 ° C annealing seems to have little or no contribution to the ferromagnetism.

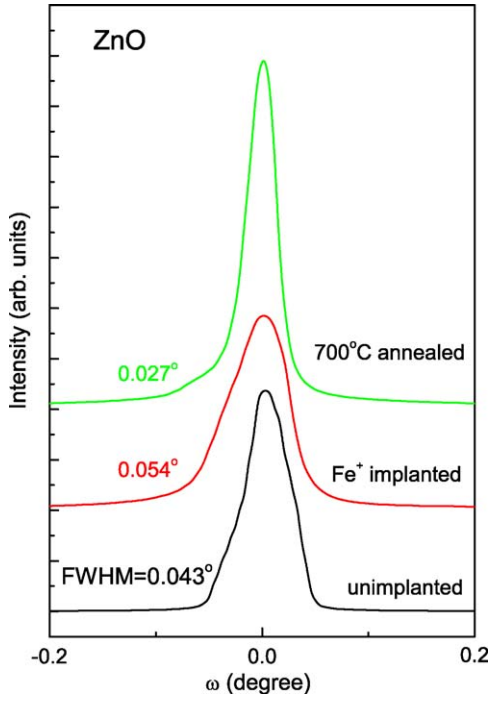

Fig. 3. The XRD ω-rocking curves of unimplanted ZnO, Fe ions implanted ZnO, and thermally annealed Fe-implanted ZnO.

Fig. 5 shows the luminescence behavior for the ZnO before and after Fe^+-implantation and annealing. The photoluminescence spectrum of unimplanted samples shows a strong near-band-edge (NBE) UV emission and a weak green emission. The position of the UV emission peak is around 3.3 eV. This is due to the recombination of free excitons. The green emission located at around 2.3 eV is probably related with some deep level defects such as V_O, V_{Zn}, or O_{Zn} [36–38]. After Fe^+-implantation, neither UV nor green emissions can be observed. It is possibly due to the Fe^+-implantation-induced defects, which act as nonradiation recombination centers. They have strong ability to compete with the UV and green emission. After annealing at 700 ° C for 30 min, both green and UV emission can be detected again. This indicates that the number of implantation-induced nonradiation recombination centers decreases due to thermal annealing. However, the intensity of UV emission peak of annealed ZnO is still rather weak, indicating that annealing temperature of 700 ° C is not high enough to remove all the implantation-induced defects. No Fe-related emission band was observed in Fig. 5 after Fe^+ implantation in ZnO.

Fig. 6 shows the Raman spectra for unimplanted samples, Fe^+-implanted samples, and thermally annealed Fe-implanted samples. In our experiment range of 200–800 cm^{-1}, we observe two vibration peaks for the unimplanted ZnO located at 331 and 437 cm^{-1}, respectively. The 331 cm^{-1} mode is due to the multi-phonon process, while the predominant 437 cm^{-1} peak is the high-frequency E_2 mode. The E_2 mode corresponds to band characteristic of the wurtzite structure of ZnO [39]. After Fe^+-implantation, the peak at 331 cm^{-1} barely changes. However, a rather broad peak at around 575 cm^{-1} appeared. This also causes a decrease of the E_2 peak. This broad peak is not related with the implanted Fe impurities, as the same peak was reported in other ion-implanted or even electron-irradiated ZnO [40–42]. Such peak was ascribed by some authors as being due to either the longitudinal optical (LO) phonon of A_1[43,44] or the LO phonon of E_1[39,45]. However, it is most probably a defect-induced mode. The LO phonon band should decrease due to lattice damage, but we got a contrary result. Therefore, this peak should be mainly a defect-induced band, as implantation would introduce large amounts of defects. These defects cut the long range order of the ZnO lattice, and break the Raman selection rule. Therefore, several phonon vibration modes which are originally forbidden in the perfect lattice begin to appear, and contribute to the broad peak at 575 cm^{-1}. After annealing at 700 °C, the broad peak at 575 cm^{-1} rapidly decreases and the E_2 peak at 437 cm^{-1} recovers. This indicates that most of the Fe^+ implantation-induced defects are annealed out, which is consistent with the XRD results. Considering that the ferromagnetism has nearly no change before and after annealing, we did not find any clear correlation between the defects and ferromagnetism in ZnO.

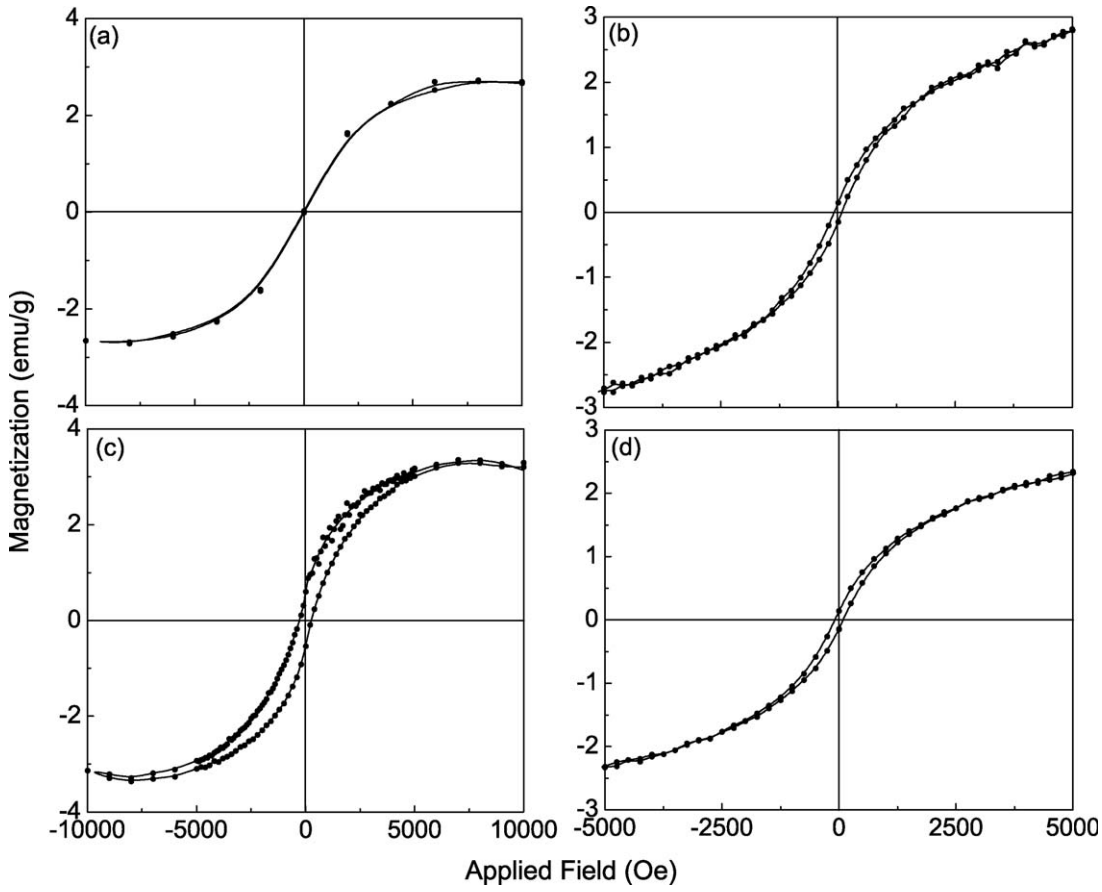

Fig. 4. The magnetization vs. applied field of as-implanted ZnO with Fe measured at (a) 300 K, (b) 250 K, and (c) 10 K. (d) The magnetization vs applied field of annealed Fe^{+}-implanted ZnO measured at 250 K.

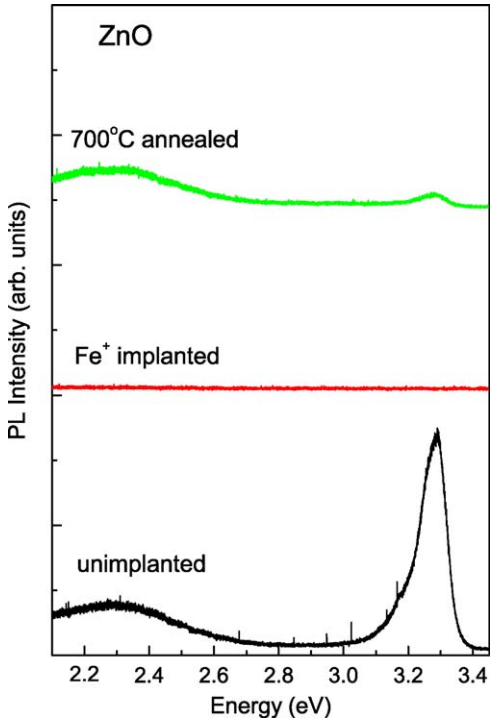

Fig. 5. PL spectra measured at room temperature for unimplanted samples, Fe ions implanted samples, and thermally annealed Fe-implanted samples.

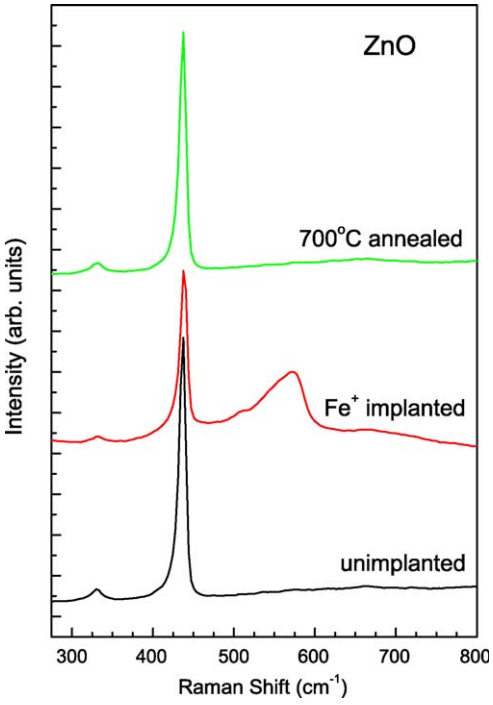

Fig. 6. Raman spectra recorded at room temperature for unimplanted samples, Fe ions implanted samples, and thermally annealed Fe-implanted samples.

4. Conclusion

In conclusion, we have studied the magnetic and structural properties of Fe^+ implanted ZnO single crystals. Various defects are introduced by implantation, which deteriorates the crystal quality of ZnO. Annealing at 700 ° C can partly remove the implantation-induced defects. Fe nanoparticles are possibly formed after thermal annealing. Ferromagnetism has been detected at or below 250 K in as-implanted samples and annealed samples. However, we did not find the correlation between Fe nanoparticles and the ferromagnetism. The Fe^+ implantation degrades the optical properties of ZnO to a large extent by the suppression of light emission due to the formation of nonradiative recombination centers. They are partly recovered after annealing at 700 °C. The implantation induced defects also affect the Raman scattering mode by produce a broad peak at around 575 cm^{-1}. Further detailed research on the defect formation and recovery in Fe^+-implanted ZnO using a slow positron beam is under consideration.

Acknowledgments

This work was supported by the Program for New Century Excellent Talents in University, the National Natural Science Foundation of China under Grant No. 10875088, and the 973 program under grant No. 2008CB617607.

References

[1] S.A. Wolf, D.D. Awschalom, R.A. Buhrman, J.M. Daughton, S. von Molnar, M.L. Roukes, A.Y. Chtchelkanova, D.M. Treger, Science 294 (2001) 1488.
[2] T. Dietl, H. Ohno, F. Matsukura, J. Cibert, D. Ferrand, Science 287 (2000) 1019.
[3] D.J. Priour, E.H. Hwang, S. Das Sarma, Phys. Rev. Lett. 92 (2004) 117201.
[4] J.M.D. Coey, M. Venkatesan, C.B. Fitzgerald, Nat. Mater. 4 (2005) 173.
[5] S.A. Chambers, Mater. Today 5 (2002) 34.
[6] A. Punnoose, K.M. Reddy, J. Hays, A. Thurber, M.H. Engelhard, Appl. Phys. Lett. 89 (2006) 112509.
[7] C. Weisbuch, B. Vinter, Quantum Semiconductor Structures: Fundamentals and Applications, Academic, San Diego, CA, 1991.
[8] K. Sato, H. Katayama-Yoshida, Jpn. J. Appl. Phys. 39 (Part 2) (2000) 555.
[9] K. Ueda, H. Tabata, T. Kawai, Appl. Phys. Lett. 79 (2001) 988.
[10] H. Saeki, H. Tabata, T. Kawai, Solid State Commun. 120 (2001) 2700.
[11] P. Sharma, A. Gupta, K.V. Rao, F.J. Owens, R. Sharma, R. Ahuja, J.M. Osorio Guillen, B. Johansson, G.A. Gehring, Nat. Mater. 2 (2003) 673.
[12] J.H. Park, M.G. Kim, H.M. Jang, S. Ryu, Y.M. Kim, Appl. Phys. Lett. 84 (2004) 1338.
[13] S. Ramachandran, A. Tiwari, J. Narayan, Appl. Phys. Lett. 84 (2004) 5255.
[14] A. Dinia, G. Schmerber, C. M"ny, V. Pierron-Bohnes, E. Beaurepaire, J. Appl. Phys. 97 (2005) 123908.
[15] G.L. Liu, Q. Cao, J.X. Deng, P.F. Xing, Y.F. Tian, Y.X. Chen, S.S. Yan, L.M. Mei, Appl. Phys. Lett. 90 (2007) 052504.
[16] M. Gacic, H. Adrian, G. Jakob, Appl. Phys. Lett. 93 (2008) 152509.
[17] X.X. Liu, F.T. Lin, L.L. Sun, W.J. Cheng, X.M. Ma, W.Z. Shi, Appl. Phys. Lett. 88 (2006) 062508.
[18] W. Yu, L.H. Yang, X.Y. Teng, J.C. Zhang, Z.C. Zhang, L. Zhang, G.S. Fu, J. Appl. Phys. 103 (2008) 093901.
[19] M. Snure, D. Kumar, A. Tiwari, Appl. Phys. Lett. 94 (2009) 012510.
[20] W. Chen, L.F. Zhao, Y.Q. Wang, J.H. Miao, S. Liu, Z.C. Xia, S.L. Yuan, Appl. Phys. Lett. 87 (2005) 042507.
[21] Z. Yang, J.L. Liu, M. Biasini, W.P. Beyermann, Appl. Phys. Lett. 92 (2008) 042111.
[22] P. Wu, G. Saraf, Y. Lu, D.H. Hill, R. Gateau, L. Wielunski, R.A. Bartynsk, D.A. Arena, J. Dvorak, A. Moodenbaugh, T. Siegrist, J.A. Raley, Y.K. Yeo, Appl. Phys. Lett. 89 (2006) 012508.
[23] W.S. Yan, Z.H. Sun, Q.H. Liu, Z.R. Li, Z.Y. Pan, J. Wang, S.Q. Wei, D. Wang, Y.X. Zhou, X.Y. Zhang, Appl. Phys. Lett. 91 (2007) 062113.
[24] V.K. Sharma, G.D. Varma, J. Appl. Phys. 102 (2007) 056105.
[25] E.-Z. Liu, Y. He, J.Z. Jiang, Appl. Phys. Lett. 93 (2008) 132506.
[26] Q. Wang, Q. Sun, G. Chen, Y. Kawazoe, P. Jena, Phys. Rev. B 77 (2008) 205411.
[27] D.P. Norton, M.E. Overberg, S.J. Pearton, K. Pruessner, J.D. Budai, L.A. Boatner, M.F. Chisholm, J.S. Lee, Z.G. Khim, Y.D. Park, Appl. Phys. Lett. 83 (2003) 5488.
[28] K. Potzger, S.Q. Zhou, H. Reuther, A. M"1cklich, F. Eichhorn, N. Schell, W. Skorupa, M. Helm, J. Fassbender, T. Herrmannsdorfer, T.P. Papageorgiou, Appl. Phys. Lett. 88 (2006) 052508.
[29] S.Q. Zhou, K. Potzger, K. Kuepper, J. Grenzer, M. Helm, J. Fassbender, E. Arenholz, J.D. Denlinger, J. Appl. Phys. 103 (2008) 043901.
[30] S.Q. Zhou, K. Potzger, J. von Borany, R. Grotzschel, W. Skorupa, M. Helm, J. Fassbender, Phys. Rev. B 77 (2008) 035209.
[31] S.Q. Zhou, K. Potzger, G. Talut, H. Reuther, J. von Borany, R. Grotzschel, W. Skorupa, M. Helm, J. Fassbender, N. Volbers, M. Lorenz, T. Herrmannsdorfer, J. Appl. Phys. 103 (2008) 023902.
[32] K. Potzger, K. Kuepper, Q. Xu, S. Zhou, H. Schmidt, M. Helm, J. Fassbender, J. Appl. Phys. 104 (2008) 023510.
[33] J.P. Biersack, L.G. Haggmark, Nucl. Instrum. Methods 174 (1980) 257.
[34] E. Rita, U. Wahl, J.G. Correia, E. Alves, J.C. Soares, Appl. Phys. Lett. 85 (2004) 4899.
[35] Z.Q. Chen, S. Yamamoto, M. Maekawa, A. Kawasuso, X.L. Yuan, T. Sekiguchi, J. Appl. Phys. 94 (2003) 4807.
[36] K. Vanheusden, C.H. Seager, W.L. Warren, D.R. Tallant, J.A. Voigt, Appl. Phys. Lett. 68 (1996) 403.
[37] Q.X. Zhao, P. Klason, M. Willander, H.M. Zhong, W. Lu, J.H. Yang, Appl. Phys. Lett. 87 (2005) 211912.
[38] B. Lin, Z. Fu, Y. Jia, Appl. Phys. Lett. 79 (2001) 943.
[39] T.C. Damen, S.P.S. Porto, B. Tell, Phys. Rev. 142 (1966) 570.
[40] Z.Q. Chen, A. Kawasuso, Y. Xu, H. Naramoto, X.L. Yuan, T. Sekiguchi, R. Suzuki, T. Ohdaira, J. Appl. Phys. 97 (2005) 013528.
[41] Z.Q. Chen, M. Maekawa, A. Kawasuso, S. Sakai, H. Naramoto, J. Appl. Phys. 99 (2006) 093507.
[42] Z.Q. Chen, S.J. Wang, M. Maekawa, A. Kawasuso, H. Naramoto, X.L. Yuan, T. Sekiguchi, Phys. Rev. B 75 (2007) 245206.
[43] C.J. Youn, T.S. Jeong, M.S. Han, J.H. Kim, J. Cryst. Growth 261 (2004) 526.
[44] X. Wang, S. Yang, J. Wang, M. Li, X. Jiang, G. Du, X. Liu, R.P.H. Chang, J. Cryst. Growth 226 (2001) 123.
[45] Y.J. Xing, Z.H. Xi, Z.Q. Xue, X.D. Zhang, J.H. Song, R.M. Wang, J. Xu, Y. Song, S.L. Zhang, D.P. Yu, Appl. Phys. Lett. 83 (2003) 1689.